Journal of ELECTRONIC MATERIALS, Vol. 47, No. 1, 2018
DOI: 10.1007/s11664-017-5770-8

Ultra-Thin Dual-Band Polarization-Insensitive and Wide-Angle Perfect Metamaterial Absorber Based on a Single Circular Sector Resonator Structure

HAO LUO[1] and YONG ZHI CHENG[2,3,4]

1.—College of Physics and Electronic Engineering, Xinyang Normal University, Xinyang 464000, People's Republic of China. 2.—School of Information Science and Engineering, Wuhan University of Science and Technology, Wuhan 430081, People's Republic of China. 3.—e-mail: chengyz@wust.edu.cn. 4.—e-mail: cyz0715@126.com

We present a simple design for an ultra-thin dual-band polarization-insensitive and wide-angle perfect metamaterial absorber (PMMA) based on a single circular sector resonator structure (CSRS). Both simulation and experimental results reveal that two resonance peaks with average absorption above 99% can be achieved. The dual-band PMMA is ultra-thin with total thickness of 0.5 mm, which is $< \lambda/38$ with respect to the operation frequencies. The surface electric field and current distributions of the unit-cell structure reveal the physical picture of the dual-band absorption. Numerical simulations demonstrate that the PMMA could retain high absorption level at large angles of polarization and incidence for both transverse electric (TE) and transverse magnetic (TM) modes. Furthermore, the absorption properties of the PMMA can be adjusted by varying the geometric parameters of the unit-cell structure.

Key words: Metamaterial absorber, dual-band, polarization-insensitive, circular sector resonator

INTRODUCTION

Metamaterials (MMs) are artificial engineered subwavelength periodic composite materials or structures, often exhibiting exotic electromagnetic (EM) or optical properties that are unavailable in Nature.[1,2] Over the past few years, MMs have become a very important research topic in science and technology due to their wide range of potential applications, e.g., as imaging lenses,[3] for negative refraction,[4–6] cloaking,[7] etc. Among these developments, perfect metamaterial absorbers (PMMAs) have received great attention and interest because of their potential applications in related optoelectronic areas, including solar cells, thermal radiation imaging, detection, and sensing.[8–11] A typical PMMA is composed of a dielectric substrate sandwiched with a metallic resonator structure and continuous metal film or wire. By adjusting the geometric parameters of the unit-cell structure of the PMMA, one can achieve near-unity absorption due to the relative impedance matching to free space.[11] PMMAs based on various structures for use in the microwave to visible region have been proposed and rapidly developed.[12–19] However, most proposed PMMAs are dependent on the angles of polarization and incidence. In many practical application areas, it is necessary to design dual- or multiband PMMAs that are polarization-insensitive and wide angle simultaneously.

Owing to the fundamental EM resonances, the number of absorption peaks depends on the number of resonant modes of the MM structure. Thus, dual-, triple-, and multiband PMMAs have been proposed and developed using multiple nondegenerate subunits within a superunit structure.[12,13,20–27] However, such multiband PMMAs based on superunit structures are complicated, thus increasing fabrication costs. In addition, many interactions can occur between their subunits, resulting in greater

(Received April 3, 2017; accepted August 28, 2017; published online September 8, 2017)

dependence on the angles of incidence and polarization of the incident EM wave. A useful approach is therefore to design dual- or multiband PMMAs by combining fundamental and higher-order resonances in a single resonator structure.[28–31] Yoo et al. proposed a dual-band PMMA with single disk/donut structure based on fundamental and third-harmonic magnetic resonances.[28] Wang et al. presented a triple-band terahertz PMMA using only an asymmetric cross structure.[29] Then, Hu et al. proposed a four-band PMMA based on a simple #-shaped resonator,[30] and Kim et al. proposed a triple-band PMMA utilizing a single rectangular hole.[31] However, the above-mentioned multiband PMMA structures are sensitive to all angles of polarization and incidence, limiting their practical applications.

We present herein a simple and effective design for a dual-band polarization-insensitive and wide-angle PMMA for use in the microwave region. Dual-band perfect absorption (over 99%) can be obtained using this single patterned structure. The PMMA is ultra-thin with thickness of only 0.5 mm. The origin of the dual-band perfect absorption is clarified by analyzing the distributions of the electric field and surface current of the unit-cell structure. The polarization angle and oblique angle of incidence dependence of the PMMA were studied numerically. Finally, we also studied the influence of the geometric parameters on the dual-band absorption properties of the PMMA.

STRUCTURE DESIGN, SIMULATION, AND EXPERIMENT

Figure 1a and b presents the simple design of the PMMA, consisting of a single metallic circular sector resonator structure (CSRS) sandwiched with a continuous metallic film and a dielectric substrate. The single CSRS contains a circular patch at the center with four circular sectors around it, similar to a previous design.[32] It can be expected that the designed PMMA will be insensitive to all polarization angles for both TE and TM modes due to the high geometric symmetry of its unit-cell structure. The optimized geometric parameters of the unit-cell structure are as follows: $p_x = p_y = 10$ mm, $t_s = 0.5$ mm, $r = 1.3$ mm, $l = 4.35$ mm, and $\alpha = 80°$. In our design, lossy copper film with conductivity of $\sigma = 5.8 \times 10^7$ S/m and thickness of 10 μm was selected for the metallic elements. FR-4 with permittivity and loss tangent of 4.3 and 0.025 was selected as the dielectric spacer.

To verify the dual-band perfect absorption behavior of this design, we performed full-wave EM simulations using the frequency solver based on the finite integration technology (FIT) in CST Microwave Studio. In these simulations, unit-cell boundary conditions were employed in x- and y-directions. The unit-cell structure was illuminated by a normally incident plane wave with electric field

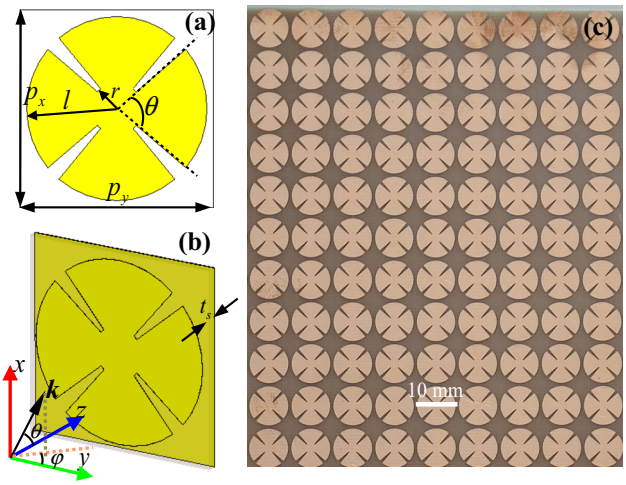

Fig. 1. Dual-band PMMA design: (a, b) front and perspective views of unit-cell structure, (c) portion of fabricated PMMA sample.

parallel to x-axis and magnetic field parallel to y-axis, with wavevector along the $+z$-axis direction.

To further verify the efficiency of the design, we fabricated a PMMA sample according to the optimized geometric parameters using conventional printed circuit board (PCB) technology. The fabricated PMMA sample (Fig. 1c) included 20 × 20 unit cells with area of 200 mm × 200 mm. In an EM anechoic chamber, two standard horn antennas connected to an Agilent N5244A PNA-X network analyzer were employed to measure the reflectance of the designed PMMA; the measurement process is detailed in Refs. 33 and 34. There was no transmission due to the continuous copper film in our design, thus only the reflectance can be examined in both the simulations and experiments. Therefore, the absorbance was calculated as $A(\omega) = 1 - R(\omega)$, where $R(\omega)$ is the reflectance as a function of frequency ω.

RESULTS AND DISCUSSION

Figure 2 shows the simulated and measured absorption spectra of the proposed PMMA in the frequency range from 3 GHz to 17 GHz. According to Fig. 2, there were two resonant frequencies, at $f_1 = 6.68$ GHz and $f_2 = 15.41$ GHz, where two absorption peaks of over 99% on average can be clearly observed. This result indicates that our designed PMMA is well impedance matched to free space at these two resonant frequencies. In addition, the designed PMMA was very thin, with thickness of about 1/89.8 and 1/38.9 of the operation wavelengths, respectively. The simulated and measured results matched reasonably well, with only slight deviations at higher frequencies due to fabrication tolerances and imperfect measurements.

To better understand the mechanism of the observed perfect absorption, the simulated distributions of the z-component of the electric field (E_z) and

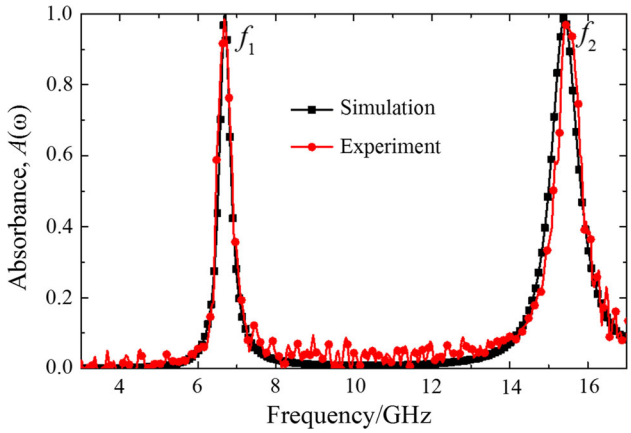

Fig. 2. Measured and simulated absorption spectra of proposed PMMA under normal incidence.

the surface current in the unit-cell structure at those two resonant frequencies are shown in Fig. 3. At the lower frequency (f_1 = 6.68 GHz), it can be observed that the electric field (E_z) distribution is mainly concentrated in the upper and lower parts of the CSRS, as shown in Fig. 3a. This enhanced electric field (E_z) distribution indicates that larger opposite charges accumulate and focus in the upper and lower parts of the CSRS. Thus, the resonant mode with lower frequency is due to the electric dipole response of the CSRS. According to Fig. 3b and c, the surface current distributions in the front and back layer were opposite, which could form a current loop between the front and back metallic layers, resulting in a strong magnetic response with fundamental *LC* resonance.[35,36] Such simultaneous excitation of the fundamental electric and magnetic resonances results in the perfect absorption at 6.68 GHz.

According to Fig. 3d, at the higher frequency (f_2 = 15.54 GHz), the electric field (E_z) distribution at the left part of the CSRS was the same as that of the right part, while the accumulated charges at the upper part of the CSRS were opposite to those of the lower part. Obviously, these characteristics of the E_z distribution reveal that this mode is the quadrupole response of the CSRS.[37,38] From Fig. 3e and f, it can be clearly observed that the surface currents are mainly concentrated in the left and right parts of the unit-cell structure, and the current flow directions in the front and back layer are also opposite. The two sub-antiparallel currents form two current loops between the front and back metallic layers, resulting in second-order magnetic response.[39] Thus, the perfect absorption at the higher frequency mainly originates from simultaneous excitation of quadrupole and second-order magnetic responses.

A simple and efficient dual-band PMMA design is therefore easily realized based on the combination of the fundamental and second-order responses of a single resonator structure, suggesting a new

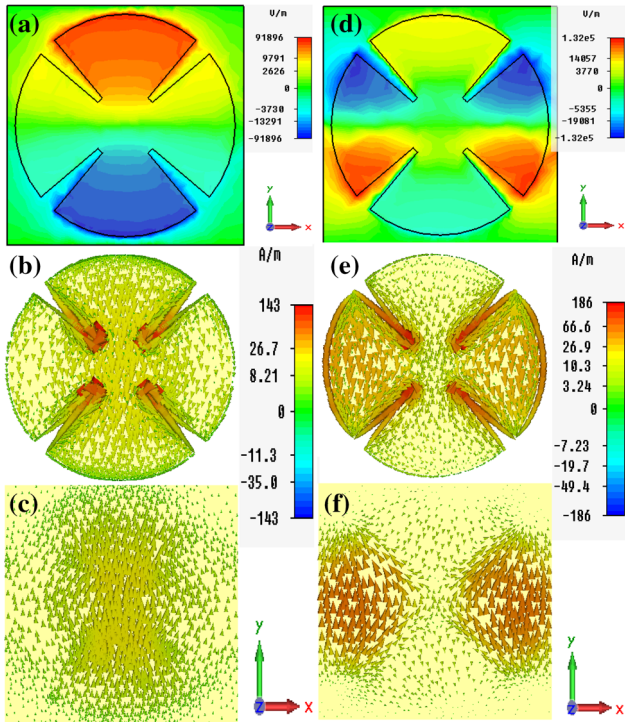

Fig. 3. (a, d) *z*-Component of electric field (E_z) and surface current distributions of (b, c) front and (e, f) back layer of unit-cell structure at different resonant frequencies: (a–c) f_1 = 6.68 GHz and (d–f) f_2 = 15.41 GHz.

approach to design dual-band PMMAs by exploring fundamental and higher-order resonance modes in a single patterned resonant structure.

To further illustrate the resonance absorption properties of the designed PMMA, we explored the distributions of the power flow stream and power loss density in the unit-cell structure. Figure 4a and c shows three-dimensional (3D) plots of the distribution of the power flow stream in the unit-cell structure at different resonant frequencies. From Fig. 4a and c, at the resonant frequencies of f_1 = 6.68 GHz and f_2 = 15.41 GHz, the input power flow stream was originally parallel in the space far from the unit-cell structure of the PMMA. As the power stream moves closer to the structure surface, most of the power that flows across the CSRS becomes curl in the dielectric substrate. However, the details for the lower and higher frequency are very different when the power stream from outside the CSRS flows into the dielectric substrate, similar to the previous structure.[34] At the lower frequency (f_1 = 6.68 GHz), the power stream from outside the area of the CSRS flows into the dielectric substrate, mainly being focused on the upper and lower edges of the unit-cell structure (Fig. 4a). At the higher frequency (f_2 = 15.41 GHz), most of the curled power stream only flows into the left and right area of the unit-cell structure (Fig. 4c). These characteristics of the power flow stream distribution further confirm that the absorptions at the lower and higher

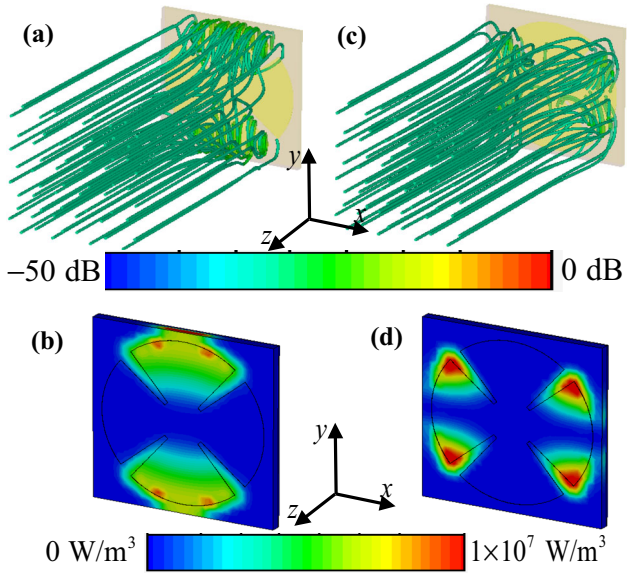

Fig. 4. (a, c) 3D distributions of power flow stream and (b, d) distributions of power loss density in the mid-plane of the unit-cell structure at resonant frequencies: (a, b) f_1 = 6.68 GHz and (b, d) f_2 = 15.41 GHz.

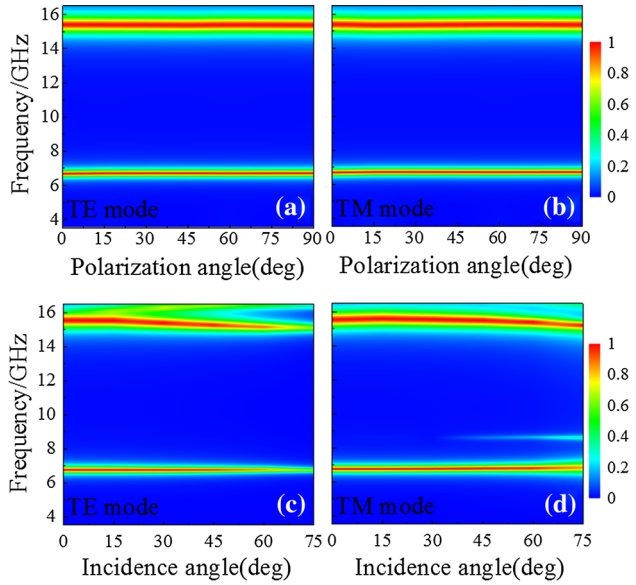

Fig. 5. Simulated absorbance for different (a, b) polarizations and (c, d) angles of incidence for different modes: (a, c) TE and (b, d) TM.

frequency are due to the fundamental and second-order responses of the proposed structure.

Figure 4b and d depicts the distributions of power loss density in the mid-plane of the unit-cell structure at the resonant frequencies. In fact, in the microwave region, it is known that the majority of incident EM wave energy will be dissipated as dielectric loss in the middle dielectric layer at the different resonance modes. As clearly shown in Fig. 4b for the lower frequency (f_1 = 6.68 GHz), the power loss is mainly focused in the upper and lower parts of the mid-plane of the unit-cell structure. Meanwhile, at the higher frequency (f_2 = 15.41 GHz), the power loss is mainly concentrated in the left and right parts of the mid-plane of the unit-cell structure. These results further confirm that the perfect absorption of the designed PMMA is due to the combination of the fundamental and second-order resonance modes.

The dependence of the PMMA on the polarization and oblique angle of incidence for both the TE and TM modes was studied numerically, as shown in Fig. 5. At normal incidence, the absorbance for different polarization angles (φ = 0° to 90°) remained unchanged for both the TE and TM modes, as shown in Fig. 5a and b. This indicates that the designed PMMA retains polarization stability under normal incidence. We also simulated the absorbance of the PMMA for different oblique angles of incidence for both the TE or TM modes. For the TE mode (Fig. 5c), it was observed that the PMMA retained high absorbance above 95% at the resonant frequencies for angle of incidence (θ) < 65°. However, for θ > 65°, the dual-band absorbance gradually decreased with increasing angle of incidence θ. This can be easily understood on the basis that the magnetic field of the incident EM wave could no longer efficiently induce the resonant currents for higher angle of incidence. In this case, the fundamental and second-order magnetic resonance cannot be excited effectively. For the TM mode (Fig. 5d), the absorbance was less affected when increasing the angle of incidence θ, since the magnetic field of the incident EM wave could still efficiently drive the antiparallel currents for all angles of incidence. It is noteworthy that additional resonance modes were observed for the TM mode at higher angle of incidence, which is associated with higher-order resonances. At higher angle of incidence (θ > 50°) for the TM mode, the split mode frequency was lower than the second-order one, because of constructive interaction due to a phase relationship.[39]

We further studied the dependence of the absorbance on various geometric parameters of the proposed PMMA design. As shown by the unit cell of the designed PMMA in Fig. 1a and b, the absorption properties are mainly determined by four geometric parameters: the center circular radius (r), the inner angle (α) of the circular sector, the circular sector radius (l), and the thickness of the dielectric substrate (t_s). Figure 6 shows the simulated absorbance for different values of these geometric parameters (r, α, l, and t_s) of the unit-cell structure. In these simulations, when changing one of the geometric parameters of the unit-cell structure, the others were fixed unchanged; For example, when changing r (to 1.0 mm, 1.5 mm, 2.0 mm, and 2.5 mm), the others were fixed as $p_x = p_y$ = 10 mm, t_s = 0.5 mm, l = 4.35 mm, and α = 80°.

As shown in Fig. 6a, when increasing r, the resonant frequencies increased while the

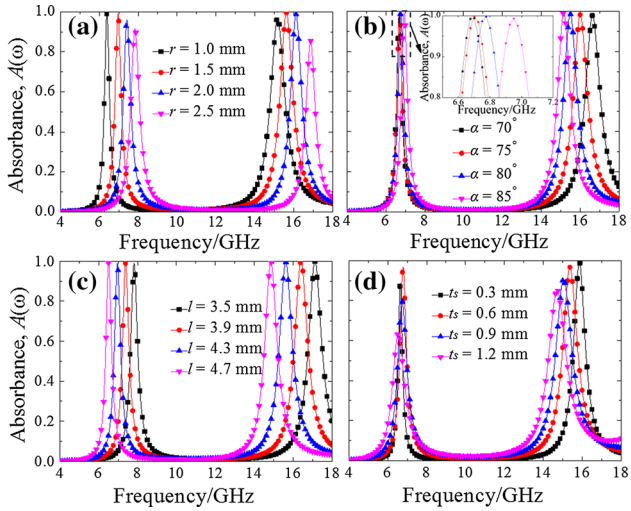

Fig. 6. Absorbance spectra of proposed PMMA when varying different geometric parameters: (a) center circular radius (r), (b) inner angle (α) of circular sector, (c) sector radius (l), and (d) thickness of dielectric substrate (t_s).

absorbance at the lower frequency decreased slightly and that at higher frequency first increased then decreased. According to LC circuit theory, the resonant frequency can be expressed as $f = \frac{1}{2\pi\sqrt{LC}}$, where the effective capacitance C and effective inductance L are mainly determined by the geometric parameters of the unit-cell structure. On increasing r, the effective capacitance C will decrease,[40,41] thus resulting in an increase of the lower and higher resonant frequencies. According to Fig. 6b, the absorbance at both the lower and higher resonant frequencies remained nearly unchanged when changing the value of α. However, the lower frequency increased slightly while the higher frequency decreased gradually when increasing α, since the C value at the lower frequency decreased slightly while that at the higher frequency gradually increased. From Fig. 6c, it can be observed that the lower and higher frequencies gradually decreased with increase of the value of l. This occurs because the L value at the lower and higher frequencies will increase, so the resonant frequencies decrease accordingly. From Fig. 6d, when increasing t_s, the lower resonant frequency remained nearly unchanged while the higher one gradually decreased. This can be understood based on the fact that the C and L values at the lower resonant frequency will remain nearly unchanged while the L value at the higher resonant frequency will increase when increasing t_s. Note that the absorption level at the lower and higher frequencies will decrease when t_s deviates from the optimal value (t_s = 0.5 mm, 0.6 mm). Thus, selection of the thickness of the dielectric substrate is very important for the operation of the dual-band PMMA.

Based on the analysis above, the resonant frequencies and absorption level were sensitive to the geometric parameters of the unit-cell structure. Thus, the dual-band absorption properties can be modified and adjusted by changing these geometric parameters.

CONCLUSIONS

An ultra-thin polarization-insensitive and wide-angle dual-band PMMA for operation in the microwave region was designed based on a CSRS placed over a ground plane with a dielectric substrate. Both simulations and experiments confirmed that the absorbance of the PMMA was above 99% on average at two different resonant frequencies. The dual-band PMMA had very low thickness (only 0.5 mm), being about 1/89.8 and 1/38.9 of the operation wavelengths, respectively. The simulated electric field and surface current distributions indicate that the dual-band perfect absorption mainly originated from the fundamental and second-order response. The proposed PMMA retained absorbance of 99% for all polarization angles of both TE and TM modes under normal incidence, while for oblique incidence, absorbance above 90% was retained for angles of incidence up to 60° for TE mode and 75° for TM mode. The dual-band absorption properties of the design can be modified and adjusted by varying the geometric parameters of the unit cell. This design provides considerable freedom to shift or change the absorption properties of the PMMA to meet different application requirements. In addition, such dual-band perfect PMMAs could easily be realized for use in other frequency ranges (e.g., radio, terahertz, infrared, and visible regions) due to its geometric scalability. Thus, it is expected that this approach could represent a simple and effective method to design novel high-performance dual- and multiband PMMAs.

ACKNOWLEDGEMENTS

This work was supported by the National Natural Science Foundation of China (Grant No. 61605147), the Science and Technology Program of Henan Province (Grant No. 142300410195), and the Natural Science Foundation of Hubei Province (Grant No. 2017CFB588).

REFERENCES

1. W. Cai and V. Shalaev, *Optical Metamaterials: Fundamentals and Applications* (New York: Springer, 2009), p. 15.
2. T.J. Cui, R.S. David, and R. Liu, *Metamaterials: Theory, Design, and Applications* (New York: Springer, 2010), p. 4.
3. P.V. Parimi, W.T. Lu, P. Vodo, and S. Sridha, *Nature* 426, 404 (2003).
4. R.A. Shelby, D.R. Smith, and S. Schultz, *Science* 292, 77 (2001).
5. N.T. Tung, V.D. Lam, J.W. Park, M.H. Cho, J.Y. Rhee, W.H. Jang, and Y.P. Lee, *J. Appl. Phys.* 106, 053109 (2009).
6. Y.Z. Cheng, Y. Nie, and R.Z. Gong, *Eur. Phys. J. B* 85, 62 (2012).
7. D. Schurig, J.J. Mock, B.J. Justice, S.A. Cummer, J.B. Pendry, A.F. Starr, and D.R. Smith, *Science* 314, 977 (2006).

8. N.I. Landy, S. Sajuyigbe, J.J. Mock, D.R. Smith, and W.J. Padilla, *Phys. Rev. Lett.* 100, 207402 (2008).
9. Y.Q. Ye, Y. Jin, and S.L. He, *JOSA B* 27, 498 (2010).
10. Y.Z. Cheng, H.L. Yang, Z.Z. Cheng, and N. Wu, *Appl. Phys. A* 102, 99 (2011).
11. C.M. Watts, X. Liu, and W.J. Padilla, *Adv. Mater.* 24, 98 (2012).
12. Z.W. Mao, S.L. Liu, B.R. Bian, B.Y. Wang, B. Ma, L. Chen, and J. Xu, *J. Appl. Phys.* 115, 204505 (2014).
13. Y. Ma, Q. Chen, J. Grant, S.C. Saha, A. Khalid, and D.R.S. Cumming, *Opt. Lett.* 36, 945 (2011).
14. Y.Z. Cheng, Y. Nie, and R.Z. Gong, *Opt. Laser Technol.* 8, 415 (2013).
15. S. Chen, H. Cheng, H. Yang, J. Li, X. Duan, C. Gu, and J. Tian, *Appl. Phys. Lett.* 99, 253104 (2011).
16. W. Ma, Y.Z. Wen, and X.M. Yu, *Opt. Express* 21, 30724 (2013).
17. D. Xiao, K.Y. Tao, and Q. Wang, *Plasmonics* 11, 389 (2016).
18. G.M. Akselrod, J. Huang, T.B. Hoang, P.T. Bowen, L. Su, D.R. Smith, and M.H. Mikkelsen, *Adv. Mater.* 27, 8028 (2015).
19. Y.Z. Cheng, X.S. Mao, C. Wu, L. Wu, and R.Z. Gong, *Opt. Mater.* 53, 195–200 (2016).
20. M. Li, H.L. Yang, X.W. Hou, Y. Tian, and D.Y. Hou, *Prog. Electromagn. Res.* 108, 37 (2010).
21. J. Lee and S, Lim. *Electron. Lett.* 47, 8 (2011).
22. X.P. Shen, Y. Yang, Y. Zang, J. Gu, and J. Han, *Appl. Phys. Lett.* 101, 154102 (2012).
23. H.X. Xu, G.M. Wang, M.Q. Qi, J.G. Liang, J.Q. Gong, and Z.M. Xu, *Phys. Rev. B* 86, 205104 (2013).
24. Y.Z. Cheng, R.Z. Gong, and Y. Nie, *Appl. Phys. B* 111, 483 (2013).
25. Y.B. Ma, H.W. Zhang, Y.X. Li, Y.C. Wang, W.E. Lai, and J. Li, *Chin. Phys. B* 23, 58102 (2014).
26. B. Yang, Z. Li, D.Q. Ju, Y.Y. Jiang, and L.H. Liu, *Opt. Express* 23, 8670 (2015).
27. A. Osman, R.K.A. Mohamad, A.M. Noor, A.S. Noor, Z. Farid, and A.M. Huda, *Appl. Phys. A* 123, 63 (2017).
28. J.Y. Young, J.K. Young, T.P. Van, Y.R. Joo, W.K. Ki, H.J. Won, Y.H. Kim, H. Cheong, and Y.P. Lee, *Opt. Express* 21, 32484 (2013).
29. B.X. Wang, G.Z. Wang, and T. Sang, *J. Phys. D Appl. Phys.* 49, 165307 (2016).
30. D. Hu, H.Y. Wang, Z.J. Tang, X.X. Zhang, and Q.F. Zhu, *Appl. Phys. A* 122, 826 (2016).
31. S.J. Kim, Y.J. Yoo, Y.J. Kim, and Y.P. Lee, *Opt. Commun.* 382, 151 (2017).
32. D.J. Lee, J.G. Hwang, D. Lim, T. Hara, and S.J. Lim, *Sci. Rep.* 6, 27155 (2016).
33. J.C. Zhao and Y.Z. Cheng, *J. Electron. Mater.* 44, 4269 (2016).
34. Y.Z. Cheng, B. He, J.C. Zhao, and R.Z. Gong, *J. Electron. Mater.* 46, 1293 (2017).
35. Y.Z. Cheng, R.Z. Gong, and Z.Z. Cheng, *Opt. Commun.* 361, 41 (2016).
36. B.X. Wang and G.Z. Wang, *Appl. Phys. Express* 10, 034301 (2017).
37. Z. Liao, Y. Luo, A.I. Fernández-Domínguez, X.P. Shen, S.A. Maier, and T.J. Cui, *Sci. Rep.* 5, 9590 (2015).
38. D. Govind and S.A. Ramakrishna, *J. Opt.* 16, 094016 (2014).
39. I. Kota, H. Toshiyoshi, and H. Iizuka, *J. Appl. Phys.* 119, 063101 (2016).
40. M. Maeda, *IEEE Trans. Microw. Theory Tech.* 20, 390 (1972).
41. Y.Z. Cheng, M.L. Huang, H. Chen, Z. Guo, X. Mao, and R. Gong, *Materials* 10, 591 (2017).